Article

Polymersome-Encapsulated Chemosensors: New Design Strategies toward Biofluid-Applicable Cucurbit[7]uril Indicator Displacement Assays

Pierre Picchetti,[||] Amanda K. Pearce,[||] Sam J. Parkinson, Laura M. Grimm, Rachel K. O'Reilly,* and Frank Biedermann*
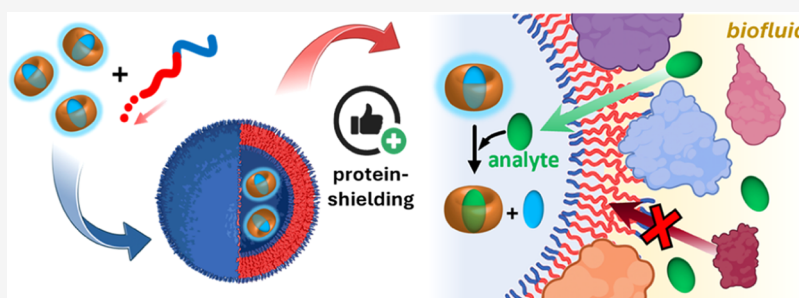
Cite This: Macromolecules 2024, 57, 4062−4071

Read Online

ACCESS | Metrics & More | Article Recommendations | SI Supporting Information

ABSTRACT: The development of supramolecular cucurbit[7]uril-based chemosensors for the detection of bioanalytes in biofluids such as untreated human serum and inside cells is a challenging task due to competition with proteins and inorganic salts. In this contribution, we show that the encapsulation of cucurbit[7]uril-based chemosensors in polymersomes can prevent deactivation, rendering the chemosensors operational in human serum and inside cells. We found that polymersomes with a hydrophilic poly-[N,N-dimethylacrylamide] corona, especially those smaller than 200 nm, exhibit greater permeability to small bioactive molecules compared with polymersomes with a bulkier poly(ethylene glycol) corona. Furthermore, analytes characterized by intermediate lipophilicity, low charge density, and a rigid structure display enhanced permeability through the polymersomes. The polymer membrane serves as a selective filter that allows small molecules to pass through a chemosensor while larger proteins are held outside the polymersome. In addition to providing a new approach for stabilizing chemosensors in protein-rich media, this study underscores the potential utility of polymersome-encapsulated chemosensors in investigating membrane permeability.

INTRODUCTION

A central challenge in developing future healthcare sensors lies in the ability to detect biomolecules at the point of care using affordable, rapid, and user-friendly assays.[1,2] Current standard instrumentation in clinical diagnostics falls short of providing comprehensive solutions to this ambitious goal. This emphasizes the appeal of supramolecular host−guest chemosensors, which function through molecular recognition, as an attractive alternative.[3,4] Among the macrocyclic receptors utilized in the design of host−guest chemosensor assays, cucurbit[n]urils (CBn)[5−7] stand out due to their exceptionally high binding affinity for a wide range of biomolecules[8−10] and drugs[11,12] in aqueous media ($K_a \approx 10^3–10^9$ M^{-1}).[13] The detection of biologically relevant small organic molecules is made possible by using a combination of CBn as a high-affinity receptor and a suitable indicator dye. Self-assembled CBn·dye complexes are employed as chemosensing ensembles in competitive binding assays, such as the indicator displacement assay (IDA).[14,15] Competitive binding assays with CBn as the

host offer versatile signal readouts, including fluorescence,[16] chemiluminescence,[17] or an electrical current.[18]

Despite their unique properties as macrocyclic receptors, bimolecular cucurbit[7]uril (CB7)-based chemosensing ensembles[14,19] (in the following referred to as chemosensors) are susceptible to deactivation in intricate, protein-rich biofluids, such as untreated serum samples, untreated urine, and within cells (Figure 1a). This is mainly due to the competition of the indicator molecules located in the host's cavity with comparably very high concentrations of inorganic cations (>5 mM)[20] and proteins (e.g., human serum albumin or insulin).[21−29] The nonspecific interaction with proteins can block the macrocycle cavity or disassemble the chemosensor,
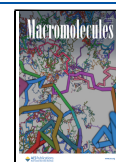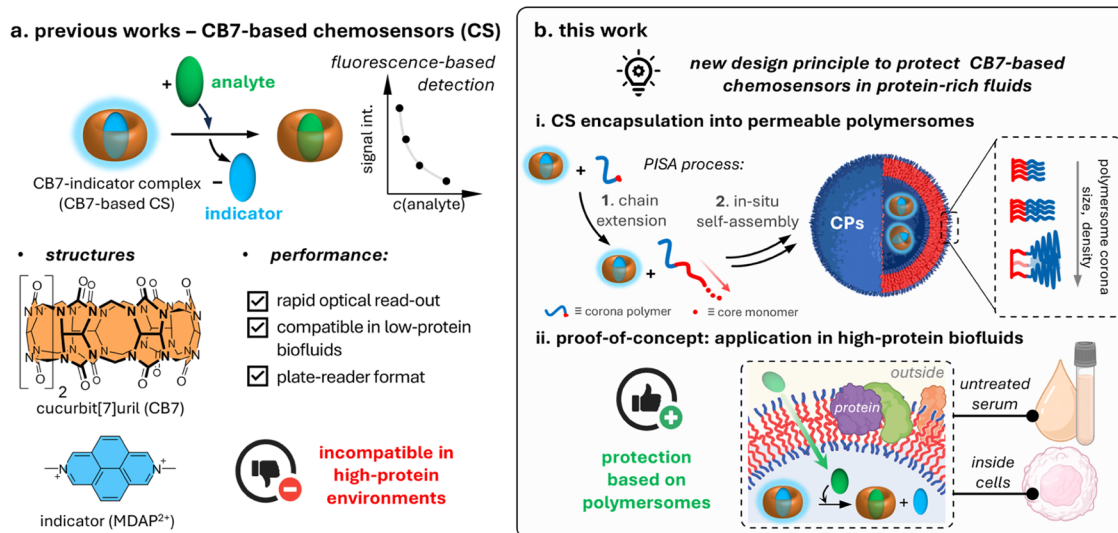
Figure 1. (a) Schematic representation of a simplified host–guest type chemosensor consisting of CB7 as the macrocyclic host and MDAP²⁺ as the luminescent indicator, depicted in an indicator displacement assay format. (b) Overview of the work presented herein. (i) The chemosensor is encapsulated in a polymersome by a water-compatible PISA process. (ii) The encapsulated chemosensor remains functional in untreated serum samples and inside cells, as the polymersome membrane effectively shields it from proteins.

e.g., by competitive binding of the indicator dye, which renders it dysfunctional for the proposed detection of small biomolecules. Although we successfully employed unimolecular CB*n*-based chemosensors that function in high-salt buffers (10× PBS) as well as in human urine and saliva,[30−32] new design principles are needed to strengthen resistance to protein-mediated deactivation. Consequently, pursuing alternative design strategies to stabilize bimolecular CB7-based chemosensors in complex biofluids remains an attractive and unsolved challenge. To render CB7-based chemosensors applicable in complex biofluids, we drew inspiration from recent reports on the liposomal encapsulation of CB*n*-based chemosensors for screening lipid membrane permeability to drugs and biogenic amines.[33,34]

We hypothesized that encapsulating chemosensors in the lumen of a vesicular nanoparticle structure, permeable to small molecules, would shield them from deactivation by proteins in biofluids (Figure 1b).

However, despite their widespread use in biological research, many liposomes are known to have low stability in biological media, making them less than ideal candidates for creating long-term stable vesicles that are largely inert to changing media composition (pH, salinity, and protein concentration).[35−38] In search of more stable vesicular structures to encapsulate a CB7-based chemosensor and protect it from its environment, we turned our attention to synthetic polymer vesicles or polymersomes.

Polymersomes consist of an aqueous core with a hydrophobic bilayer membrane and are formed by the self-assembly of amphiphilic block copolymers, usually synthesized through living polymerization processes.[39−41] Furthermore, vesicular nanoparticles can be prepared *in situ* via reversible addition−fragmentation chain transfer (RAFT) and polymerization-induced self-assembly (PISA),[42] thereby circumventing otherwise laborious multistep polymerization and assembly processes. The final morphology of the polymersomes can be adjusted by the relative volume fractions of the hydrophilic and hydrophobic block units and by the weight fraction of the reactants in the polymerization solution.

Polymersomes have advantageous physicochemical properties compared with lipid-based nanoparticles and other self-assembled polymer structures. These include high mechanical strength,[39] chemical modularity,[43−45] and the ability to be degraded on demand[46−49]—all features that have made them attractive for drug delivery applications.[50,51]

Strategies to adjust polymersome permeability hinge on adjusting the chemical composition of the amphiphilic polymers and employing membrane cross-linkers, channel-forming proteins, or nucleic acid-based pores.[52−56] Due to their unique permeability and robustness, polymersomes have been explored as reaction vessels in biocatalysis,[55,57−61] where encapsulated enzymes are shielded from potentially denaturing environments. Furthermore, polymersomes are a subject of ongoing research in nonbiocatalysis[62−64] and bioimaging, such as pH bioimaging[65] or the detection of adenosine triphosphate.[66] Previous work has demonstrated that polymersomes inherently permit the permeation of small organic molecules while effectively excluding larger proteins.[55,67]

Despite their advantageous properties, polymersomes have not yet been employed to protect synthetic supramolecular chemosensors, such as those based on CB*n*, from challenging biological environments.

In this study, we introduce a novel design principle to protect CB7-based chemosensors by encapsulating them within polymersomes, resulting in chemosensor-loaded polymersomes (CPs, Figure 1b). Specifically, we encapsulated the CB7⊃2,7-dimethyldiazapyrenium (CB7⊃MDAP²⁺)[68,69] chemosensor ensemble within various polymersomes to circumvent its protein-induced deactivation in untreated serum samples. Moreover, we demonstrate that our approach yields CPs that retain their functionality even within cells. Finally, the use of CB7-based chemosensors offers a novel tool for directly studying the permeability of polymersome membranes to biomolecules and drugs, a crucial aspect for future evaluation and application of such vesicular and polymeric structures.[67]
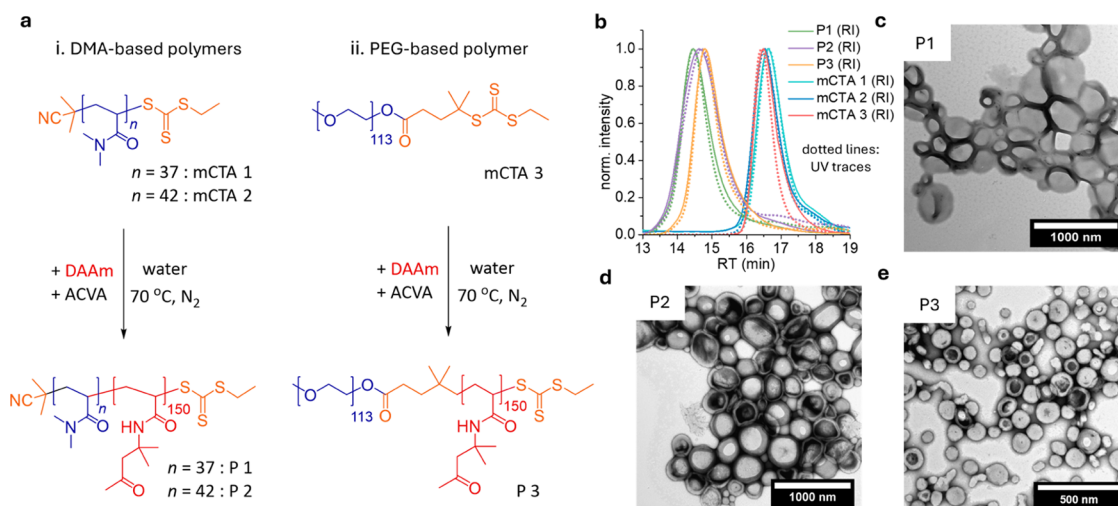
Figure 2. (a) Reaction scheme for synthesizing polymersomes (P1−P3) using aqueous PISA. (b) SEC analysis showing the refractive index (RI) and UV (309 nm) traces for mCTAs and polymersomes. TEM images of polymersomes (c) P1, (d) P2, and (e) P3.

■ RESULTS AND DISCUSSION

Preparation of Model Polymersomes and CPs. Our first goal was to synthesize three model polymersome formulations, each exhibiting vesicular and spherical morphologies with different sizes and corona compositions, using a RAFT-mediated PISA strategy. This approach was based on poly-[N,N-dimethylacrylamide]-b-poly-[diacetone acrylamide] (pDMA-pDAAm) or polyethylene glycol (PEG113)-pDAAm block copolymers, and adapted from previously reported procedures (Figure 2a, see the Supporting Information).[70,71]

The prepared polymersomes, all based on a poly-[diacetone acrylamide] (pDAAm) core, varied in the composition of their hydrophilic corona, ranging from less dense poly-[N,N-dimethylacrylamide] (pDMA) of different lengths to densely packed polyethylene glycol (PEG). The pDAAm core ensures compatibility with aqueous PISA,[72] while pDMA and PEG are well-established corona compositions that are highly hydrophilic.

The pDMA macrochain transfer agents (mCTA1 and mCTA2, Figure 2a) were synthesized using RAFT solution polymerization of DMA in 1,4-dioxane with 2,2′-azobis(2-methylpropionitrile) (AIBN) as the thermal radical initiator (see the Supporting Information for details) and S-2-cyano-2-propyl-S′-ethyl trithiocarbonate (CPEA) as the chain transfer agent, with characterization data in Table S1. Both polymerizations were quenched at conversions >90%, as was determined by ¹H NMR (Figures S1−S4), achieving a final degree of polymerization (DP) of 37 (mCTA1) and 42 (mCTA2). Size-exclusion chromatography (SEC, Figure 2b) analysis confirmed that the mCTAs had a number-average molar mass (M_n) of 5.0 and 6.1 kDa, respectively, with dispersity ($Đ_M$) below 1.2. Importantly, the SEC traces showed good overlap of the refractive index (RI) and UV (at 309 nm; trithiocarbonate group) traces, highlighting the excellent end group fidelity on the mCTAs (Figure 2b). The PEG macroCTA (mCTA3) was prepared from PEG113 monomethyl ether and 4-cyano-4-(((ethylthio)carbonothioyl)thio)-pentanoic acid (CPEPA; see the Supporting Information for details and characterization data in Table S1). ¹H NMR spectroscopy (Figure S5), RI, and UV-SEC traces (309 nm, Figure 2b) confirmed quantitative coupling, with no unfunctionalized PEG remaining.

Subsequently, thermally activated aqueous RAFT-mediated PISA was performed using 4,4′-azobis-4-cyanovaleric acid (ACVA) as the thermal radical initiator and DAAm as the hydrophobic nucleating monomer (molar ratio mCTA/DAAm = 1:150) to target a spherical vesicular morphology of empty model polymersomes (P1, P2, and P3; see the Supporting Information). Complete conversion (>97%) of the DAAm core monomer was observed after 2 h of reaction time, as assessed by NMR spectroscopy (Figures S6−S10). The resulting polymersome dispersions were purified by dialysis against water and then characterized by ¹H NMR spectroscopy, SEC, transmission electron microscopy (TEM), and dynamic light scattering (DLS).

SEC analysis confirmed quantitative blocking efficiency with number-average molar masses (M_n) of 40 kDa for P1 (synthesized using mCTA1), 30 kDa for P2 (synthesized using mCTA2), and 19 kDa for P3 (synthesized using mCTA3) with dispersity values ($Đ_M$) below 1.3 (Figure 2b; see Table S1). TEM analysis confirmed the presence of their vesicular morphology (Figure 2c−e), with DLS data showing a hydrodynamic diameter (D_h) of 392, 407, and 163 nm for P1, P2, and P3, respectively (Figures S11−S13; see Table S2).

Next, our objective was to encapsulate CB7⊃MDAP²⁺ in all polymersome formulations. To achieve this, the PISA process was performed, as previously described, but with the addition of CB7⊃MDAP²⁺ (final concentration in the reaction solution was approximately 300 μM) to the monomer mixture prior to polymerization (see the Supporting Information for details).

The resulting chemosensor-loaded polymersomes, i.e., CP1, CP2, and CP3, were purified by dialysis (molecular weight cutoff: 10 kDa) against water to remove residual and nonencapsulated species.

DLS analysis CP1 indicated a single particle distribution with D_h = 468 nm (Figure 3a), which is slightly larger than that of control P1 without the chemosensor (D_h = 392 nm). The vesicular morphology was confirmed by TEM analysis (Figure 3b). For CP2, DLS analysis of the purified samples revealed a bimodal size distribution, especially in the number-weighted intensity distribution (Figure 3c), with a vesicular structure confirmed by TEM (Figure 3d). The bimodal size distribution observed for CP2 is attributed to the presence of a small fraction of polymeric micelles in the final formulation.
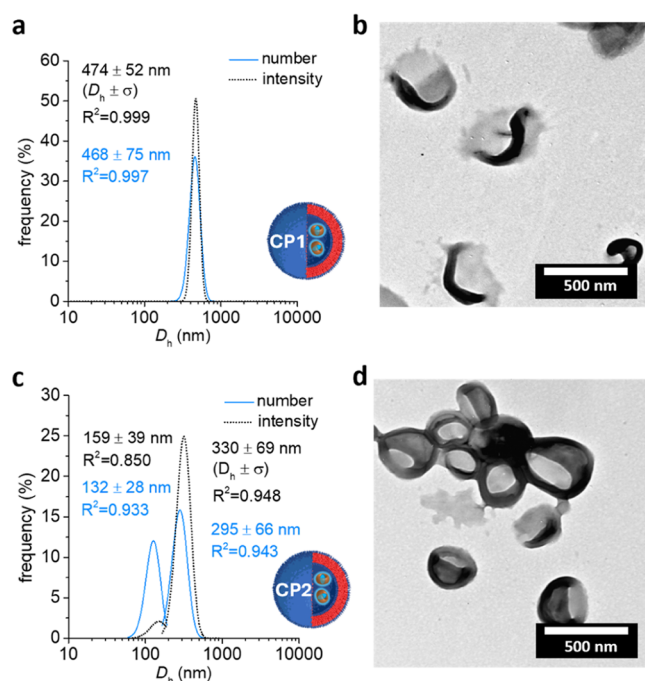
Figure 3. DLS size distribution analysis of chemosensor-loaded polymersomes: (a) CP1 and (c) CP2. TEM image of (b) CP1 and (d) CP2.

However, the predominant population comprised vesicles with an average D_h of 295 nm. For CP3, DLS analysis revealed a single population with D_h = 144 nm (Figure S14), which showed a vesicular morphology in TEM analysis (Figure S15). The DLS analysis of the pDMA and PEG corona CPs also showed that the hydrodynamic size of the polymersomes is not affected by varying pH from 4 to 8.5 (Figure S16).

Fluorescence Response Studies of CPs. Next, we investigated whether the CB7⊃MDAP²⁺ chemosensor ensemble remains active once it is encapsulated in polymersomes. We tested this by setting up an IDA with CP1, CP2, and CP3 (see the Supporting Information). We chose amines and steroids as representative analytes due to their occurrence in biofluids, such as blood, and their importance as biomarkers or pharmaceutical compounds (Figure 4a). Concretely, we have selected amantadine (Ada) as a primary amine and antidyskinetic drug used to treat Parkinson's disease[73] and influenza.[74] The selected polyamines spermine (Spe) and cadaverine (Cad) are biomarkers for cardiovascular diseases[75] and bacterial infections,[76] respectively. We were also interested in the detection of the lipophilic steroid nandrolone (Nan), a common synthetic anabolic steroid used in illegal doping preparations.[77] The analytes studied here differ in their hydrophilicity, lipophilicity (indicated by the partition coefficient, $\log P$), conformational freedom (flexibility), number of hydrogen-bonding donor−acceptor groups, and
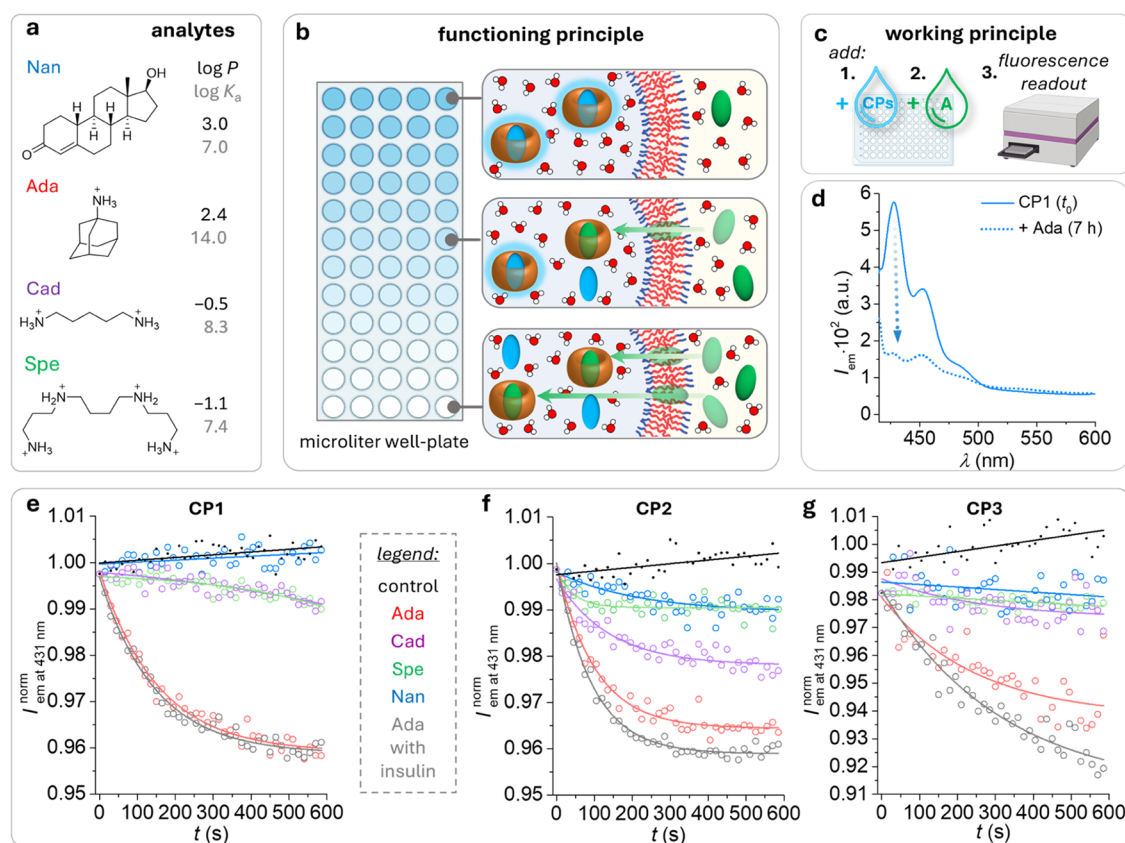
Figure 4. (a) Chemical structures and physicochemical properties of nandrolone (Nan), amantadine (Ada), cadaverine (Cad), and spermine (Spe). (b) Schematic representation of the functioning principle of CP-based chemosensors. (c) Schematic representation of the working principle of the assay. (d) Emission spectra of CP1 before and after the addition of Ada. Time-dependent fluorescence response curves for (e) CP1, (f) CP2, and (g) CP3 in the presence of analytes. As a control, CP dispersed in water without adding an analyte was used. In all emission-based experiments, the concentration of CP was 0.8 mg·mL⁻¹ (corresponding to [CB7⊃MDAP²⁺] = 0.1 μM per well), while the final concentration of the added analytes was 20 μM. All time-dependent fluorescence intensities were recorded at λ_{em} = 431 nm (λ_{ex} = 395 nm).

binding affinity to CB7 (Figure 4a). Ada (log $K_{a,CB7}$ = 14.0)[78] represents a positively charged and conformationally rigid analyte with moderate lipophilicity (log P_{Ada} = 2.4)[79] that has a single H-bond donor moiety. The two polyamines, Cad (log $K_{a,CB7}$ = 8.3)[19] and Spe (log $K_{a,CB7}$ = 7.4),[80] are multicharged and flexible chain-like molecules with two or three H-bond donor groups, respectively. Both are hydrophilic analytes, with Cad and Spe having a log P_{Cad} = −0.5 and log P_{Spe} = −1.1, respectively.[81] Nan (log $K_{a,CB7}$ = 7.0),[82] in contrast, is uncharged, flat, and has limited conformational freedom. It is also the most lipophilic analyte we studied (log P_{Nan} = 3.0),[83] bearing one H-bond donor and two acceptor groups.

We anticipated that analytes capable of crossing the polymersome membrane would reach the chemosensor in the lumen of the polymersome and displace the fluorescent indicator (MDAP^{2+}) from the CB7 cavity (Figure 4b). In such a scenario, a decrease in the fluorescence intensity is expected. To evaluate the advantages of chemosensor encapsulation using polymersomes, we chose to use a diluted CP dispersion with an apparent concentration of CB7⊃MDAP^{2+} at 0.1 μM (Figure S17), which was much lower than previously used for this chemosensor (e.g., 25 μM).[69] In fact, the high effective molarity that can be reached by the encapsulation of bimolecular chemosensors in polymersomes is another advantage of our design strategy, as it prevents the spontaneous disassembly of noncovalently bound macro-cycle−dye complexes in dilute solution.

The schematic working principle of our CP assay is depicted in Figure 4c (see the Supporting Information for details). Briefly, a dispersion of CP1, CP2, or CP3 (c_{CP2} = 0.8 mg·mL^{-1}; corresponding to an apparent concentration of 0.1 μM CB7⊃MDAP^{2+}) was added to a microliter well, to which a solution containing the analyte ($c_{analyte}$ = 20 μM) was subsequently added. After the dispersions were briefly mixed, the time-dependent fluorescence intensity (λ_{ex} = 395 nm, λ_{em} = 431 nm) was recorded. Fluorescence intensity (I_{rel}) curves were normalized to the blank value and aligned to start at the same intensity at t_0 (start of data acquisition by the instrument). The analyte concentrations were chosen to be within biologically plausible concentrations.

The addition of Ada to CP1 dispersed in water caused a slow but steady decrease in the emission intensity over time (Figures 4d and S18). This outcome aligned with our expectation that the translocation of the analyte into the lumen of the polymersome, driven by a concentration gradient, is feasible. In contrast to the addition of Ada to CB7⊃MDAP^{2+} in solution (no polymersome), for which the emission readout equilibrates within minutes,[69] this process extended over several hours for CP-encapsulated CB7⊃MDAP^{2+}. This prolonged duration can be attributed to the slow permeation of Ada through the membrane.

We recorded the time-resolved emission response of CP1, CP2, and CP3 in water upon introducing 20 μM of each analyte (Ada, Cad, Spe, Nan) to investigate the factors that affect membrane permeability. For this purpose, the signal response curves were analyzed for up to 10 min (600 s). This time range was chosen because the intensity curves follow a monoexponential decay behavior in this time range, and the signal changes are distinguishable within this period. By fitting the observed fluorescence response to a monoexponential decay function, we calculated the time required for the fluorescence intensity to decrease by 50% (I_{50}). This metric

was then used to compare the analyte response times of the CPs.

First, the response curves of CPs in the presence of Ada are discussed (Figure 4e−g). Ada showed the fastest fluorescence response among all of the analytes tested. The temporal response of CPs to Ada followed the trend CP2 (I_{50} = 69 s) > CP1 (I_{50} = 151 s) > CP3 (I_{50} = 218 s). In the case of pDMA-based CPs, i.e., CP1 and CP2, CP2 displayed a significantly faster response to Ada. This enhanced responsiveness could be attributed to the smaller size of CP2 (D_h = 295 nm) compared to that of CP1 (D_h = 468 nm), resulting in a higher effective concentration of CB7⊃MDAP^{2+} in its lumen. This, in turn, promotes a more efficient binding interaction between the analyte and the chemosensor, as was discussed in the literature for other systems.[84,85] Among all CPs tested, CP3 (D_h = 144 nm), which is smaller than CP2, responded the slowest to Ada and showed a small yet distinct response to Cad, Spe, and Nan. This lower responsiveness and the slower kinetics are likely a consequence of the densely arranged polyethylene glycol corona. Subsequently, we investigated the diffusion properties of analytes other than Ada by monitoring the emission quenching when mixed with CPs. When comparing CP1 and CP2, both featuring a pDMA corona, only CP2 exhibited a clear and distinguishable emission response to all analytes tested (Figure 4f).

The strength of the emission responses of CP2 decreased in the following order: Ada > Cad > Spe > Nan. In contrast, only weak emission quenching was observed for the combination of CP1 with the polyamines Cad and Spe. Using polymersome CP3, which has a PEG corona, no analyte other than Ada-induced significant emission quenching. Control experiments with CB7⊃MDAP^{2+} alone showed that the chemosensor elicited a significantly faster fluorescence response to all analytes tested (Figure S19). It is important to note, however, that a direct comparison between the response curves of CPs and nonencapsulated CB7⊃MDAP^{2+} is not feasible. Even with adjusting the overall concentration of CB7⊃MDAP^{2+} to be the same for the CPs and the nonencapsulated chemosensor control, one cannot reach a truly comparable situation for the CPs. This is because there is a high local concentration of CB7⊃MDAP^{2+} in the lumen of CPs, whereas, for the control, partial dissociation of the bimolecular chemosensor into its host and dye components occurs in the bulk solution at the overall low micromolar concentration level (because of otherwise occurring inner filter effects, it was not possible to raise the bulk chemosensor concentration any further). Nevertheless, the results obtained clearly show that the presence of a polymeric membrane significantly helps to tune the chemosensor response.

Next, we investigated whether the CPs are functional in the presence of insulin (see the Supporting Information for details) because nonencapsulated CB7-dye chemosensors strongly respond to this protein due to their high affinity to insulin's N-terminal Phe residue.[21−26] Indeed, we found that insulin at typical plasma concentrations (c_{Ins} = 200 μg·mL^{-1})[86] did not adversely affect the response of CP1, CP2, and CP3 to Ada (Figure 4e−g, gray curves). Furthermore, the I_{50} values of the emission remained comparable to those of the case, in which there was no insulin present, with I_{50} (CP1, Ada + Ins) = 101 s and I_{50} (CP2, Ada + Ins) = 61 s. Combined with the observation that our chemosensor is deactivated by insulin in the absence of the polymersome (Figure S20), these findings show that the polymersome membrane effectively hinders the
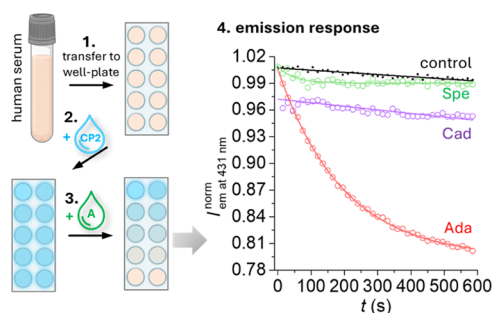
Figure 5. Fluorescence response of CP2 (0.8 mg·mL^{-1}, corresponding to [CB7⊃MDAP^{2+}] = 0.1 μM) to analytes (20 μM) in untreated human serum (λ_{ex} = 395 nm).

diffusion of proteins into the lumen of the vesicle. Together, these observations confirm the successful encapsulation of the chemosensor. Serum albumins, including bovine serum albumin (BSA), human serum albumin (HSA), and insulin, constitute a category of proteins that impair the efficacy of CB7-based chemosensing ensembles by sequestering the macrocycle–dye complex within their protein pockets.[21−29]

Pleasingly, Ada sensing experiments in untreated (non-deproteinized) human serum samples confirmed that our polymersome-encapsulated chemosensors retain their responsiveness (Figure 5), verifying that any undesirable interaction of blood proteins, such as HSA, with the chemosensor can be effectively prevented by using CPs.

Chemosensor-Loaded Polymersomes for Intracellular Imaging of Relevant Analytes. Our final goal was to investigate the applicability of CPs in a particularly intricate and protein-rich environment, such as the interior of a cell. To this end, we focused our attention on the detection of two analytes: Ada, chosen for its high binding affinity toward CB7

and as a representative model drug for Parkinson's disease, and phenylalanine (Phe, log $K_{a,CB7}$ = 6.3; log P_{Phe} = −1.7),[87,88] serving as a representative amino acid associated with phenylketonuria (Figure 6b).[89,90]

Regarding the CPs to be studied for imaging applications, we chose CP2 and CP3. CP2 was selected due to its low I_{50} value in water and its ability to retain functionality in nondeproteinized serum. CP3 was chosen because we anticipated that it would have favorable physicochemical properties for cell imaging applications compared to pDMA-based CPs. It is also the smallest chemosensor-loaded polymersome ($D_{h,CP3}$ = 144 nm) in the series, which we expected to enable faster cellular uptake (rapid internalization of particles below 200 nm has been well-described).[91] Additionally, the PEG corona protects against protein fouling and increases stability in protein-rich intracellular environments.[92]

To prove that chemosensor-loaded polymersomes can be internalized by cells, we labeled CP2 with the red-emissive dye Cy5 and incubated it with A549 cells (see the Supporting Information). After 15 min, the medium was removed, and the cells were washed several times with a phenol red-free cell culture medium and subsequently imaged using confocal microscopy. The acquired confocal microscopy images confirmed that CP2 was successfully internalized in the time frame investigated. Imaging through the Cy5 filter (at 640 nm, Figure 6a(ii)) showed punctate staining consistent with internalization through an endocytic pathway and, therefore, endosomal localization of CP2. Significantly, imaging through the MDAP^{2+} filter (488 nm, Figure 6a(iii)) displayed the presence of punctate staining, which can be superimposed with the Cy5 channel, resulting in a merged image with a yellow hue (Figure 6a(iv)). This confirmed that CB7⊃MDAP^{2+} can be trafficked into the cells by the polymersomes. Furthermore,
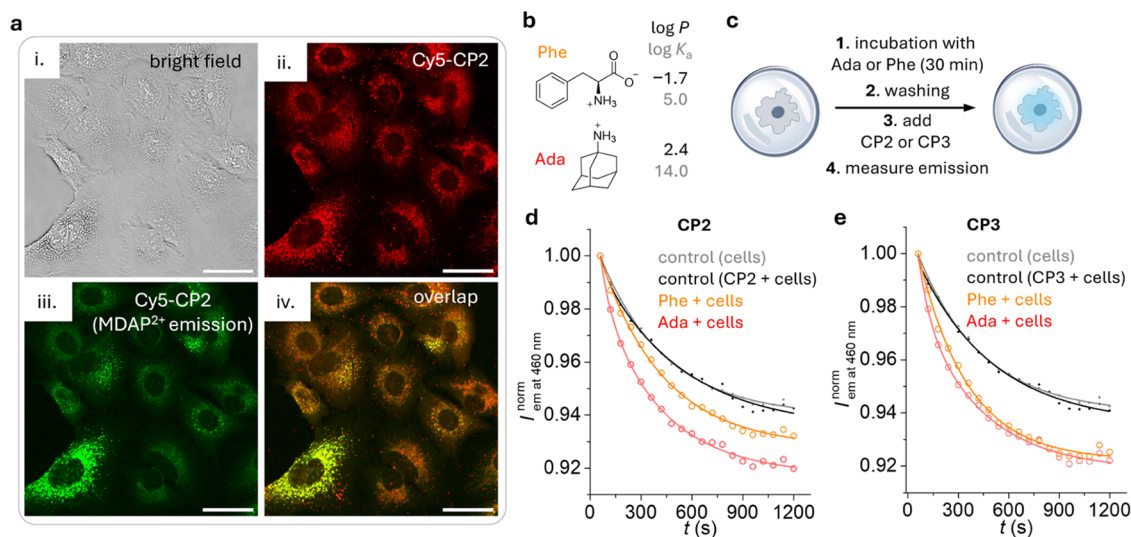
Figure 6. (a) Confocal microscopy images of A549 cells incubated with CP2 (0.5 mg·mL^{-1}) for 15 min, showing (i) brightfield, (ii) Cy5 (640 nm filter), (iii) MDAP^{2+} (488 nm filter), and (iv) a merge of the Cy5 and MDAP^{2+} channels. Scale bar = 20 μm. (b) Chemical structures of amantadine (Ada) and phenylalanine (Phe). (c) Schematic representation of the working principle of the CP-based assay in the cells. Time-dependent fluorescence response curves of (d) CP2 and (e) CP3 in A549 cells (λ_{ex} = 355 nm, λ_{em} = 460 nm). The fluorescence response curves were normalized to the blank value and aligned to start at the same intensity at t_0 (start of data acquisition by the instrument). Shown are measurements with cells alone (black trace) and with cells incubated with CPs (gray trace) only as well as analyte-dependent response curves of Ada-enriched cells (red trace) or Phe-enriched cells (orange trace) after incubation with CPs (c_{CPs} = 0.5 mg·mL^{-1}). Note that the fluorescence emission in the control (gray trace) decreases with time, which is due to the presence of phenol red in the cell culture medium, a pH indicator that is subject to photobleaching.

cytotoxicity studies (see the Supporting Information) showed that neither CP2 nor CP3 showed acute cytotoxicity at the concentrations used for the cell experiments (0.5 mg·mL^{-1}; Figure S21).

Next, we developed a cell model for the intracellular accumulation of Ada and Phe in A549 human lung epithelial cancer cells and their subsequent detection by CPs (Figure 6c; see the Supporting Information for details). Briefly, cells were incubated for 30 min with 200 μM Ada or Phe before the sensing assay was initiated by replacing the medium with fresh CP2- or CP3-containing medium (c_{CPs} in the medium was 0.5 mg·mL^{-1}). The fluorescence response was monitored (λ_{ex} = 355 nm, λ_{em} = 460 nm) every minute for 20 min (Figure 6d,e). As control experiments, cells that were enriched with either Ada or Phe but not incubated with CPs were used. In addition, a control consisting exclusively of cells was used for comparison. Note that the concentrations of Ada or Phe used for the analyte enrichment in cells were chosen based on prior cell viability assays (see the Supporting Information for details), ensuring that the analytes induced no toxicity (Figure S22).

In all experiments, a steady decrease in fluorescence emission was observed over time due to the presence of the phenol red in the cell culture medium, a standard pH indicator used to monitor optimal cell growth, which is also partially excited and subjected to photobleaching during the experiment (Figure 6d,e).

However, pleasingly, we observed an obvious larger decrease in fluorescence intensity for the cells that had both the analyte and polymersomes present inside, indicating that the CB7⊃MDAP^{2+} chemosensor remained active in this complex environment (Figure 6d,e, red and orange traces). Furthermore, the rapid cellular uptake of our CPs and the lack of red fluorescence from noninternalized polymersomes after only 15 min of incubation (Figure 6a) suggest that the observed decrease in emission signal is due to intracellular analyte binding processes.

In the case of CP2, the I_{50} values for the response to Ada increased 2.3-fold (I_{50} = 192 s) compared with the previous results obtained in water, indicating a significant decrease in performance. CP2 also showed a response in the presence of Phe (I_{50} = 260 s), which differed from the control experiments. Compared to the response obtained with Ada, the I_{50} value of CP2 is higher for Phe, possibly because this analyte has a lower binding affinity to CB7 than Ada, or because Phe's membrane translocation rate constant is lower than that of Ada, or both. Interestingly, CP3 showed a comparable performance to CP2 (Figure 6e) for both Ada (I_{50} = 181 s) and Phe (I_{50} = 205 s). This observation confirms the above-mentioned physicochemical advantages of polymersomes with a size of less than 200 nm in combination with an antiprotein fouling corona composition.

CONCLUSIONS

This work describes the successful development of CB7⊃MDAP^{2+} chemosensor-loaded polymersomes, which are functional in biological environments. The semipermeable polymer membrane, in which the chemosensors are encapsulated, acts as a molecular sieve and provides protection against protein-mediated deactivation. Notably, polymersomes with a pDMA corona are advantageous for detecting bioactive molecules and drugs in aqueous dispersions, while PEG-based polymersomes offer better robustness for cell-based

imaging applications. The encapsulation strategy presented in this contribution introduces new design strategies to improve the selectivity of host–guest chemosensors without the need for complex chemical functionalization procedures of the macrocyclic receptors. Finally, we anticipate that using different polymersome formulations with different permeabilities for small molecules holds great potential for innovative differential sensing strategies.

■ ASSOCIATED CONTENT

Ⓢ Supporting Information

The Supporting Information is available free of charge at https://pubs.acs.org/doi/10.1021/acs.macromol.3c02486.

> Full protocols, descriptions, and supporting figures, as well as information about the data uploaded to open repositories. (PDF)

■ AUTHOR INFORMATION

Corresponding Authors

Rachel K. O'Reilly − *School of Chemistry, University of Birmingham, Edgbaston, Birmingham B15 2TT, United Kingdom;* ⓞ orcid.org/0000-0002-1043-7172; Email: r.oreilly@bham.ac.uk

Frank Biedermann − *Institute of Nanotechnology (INT), Karlsruhe Institute of Technology (KIT), 76131 Karlsruhe, Germany;* ⓞ orcid.org/0000-0002-1077-6529; Email: frank.biedermann@kit.edu

Authors

Pierre Picchetti − *Institute of Nanotechnology (INT), Karlsruhe Institute of Technology (KIT), 76131 Karlsruhe, Germany;* ⓞ orcid.org/0000-0002-0689-5998

Amanda K. Pearce − *School of Chemistry, University of Birmingham, Edgbaston, Birmingham B15 2TT, United Kingdom; Department of Chemistry, Loughborough University, Leicestershire LE11 3TU, United Kingdom;* ⓞ orcid.org/0000-0003-3372-7380

Sam J. Parkinson − *School of Chemistry, University of Birmingham, Edgbaston, Birmingham B15 2TT, United Kingdom*

Laura M. Grimm − *Institute of Nanotechnology (INT), Karlsruhe Institute of Technology (KIT), 76131 Karlsruhe, Germany;* ⓞ orcid.org/0000-0002-1808-2206

Complete contact information is available at:
https://pubs.acs.org/10.1021/acs.macromol.3c02486

Author Contributions

$^{\parallel}$P.P. and A.K.P. contributed equally. This manuscript was written through the contributions of all authors.

Notes

The authors declare no competing financial interest.

■ ABBREVIATIONS

A549, adenocarcinomic human alveolar basal epithelial cells; ACVA, 4,4′-azobis-4-cyanovaleric acid; Ada, amantadine;

AIBN, 2,2′-azobis(2-methylpropionitrile); Cad, cadaverine; CB7, cucurbit[7]uril; CP, chemosensor-loaded polymersomes; CPEA, S-2-cyano-2-propyl-S′-ethyl trithiocarbonate; CPEPA, 4-cyano-4-(((ethylthio)carbonothioyl)thio)pentanoic acid; CyS, cyanine5; D_h, hydrodynamic diameter; DLS, dynamic light scattering; $Đ_M$, dispersity; DP, degree of polymerization; I_{50}, time in which the fluorescence response drops by 50%; IDA, indicator displacement assay; Ins, insulin; kDa, kilodalton; log P, partition coefficient; K_a, affinity constant; mCTA, macro-chain transfer agent; kDa, kilodalton; MDAP^{2+}, 2,7-dimethyldiazapyrenium; Nan, nandrolone; pDAAm, poly-[diacetone acrylamide]; pDMA, poly-[N,N-dimethylacrylamide]; PEG, polyethylene glycol; PISA, polymerization-induced self-assembly; RAFT, reversible addition−fragmentation chain transfer; RI, refractive index; RT, retention time; Spe, spermine; TEM, transmission electron microscopy; UV, ultraviolet

■ REFERENCES

(1) Gubala, V.; Harris, L. F.; Ricco, A. J.; Tan, M. X.; Williams, D. E. Point of Care Diagnostics: Status and Future. *Anal. Chem.* **2012**, *84*, 487−515.

(2) Reddy, B., Jr.; Hassan, U.; Seymour, C.; Angus, D. C.; Isbell, T. S.; White, K.; Weir, W.; Yeh, L.; Vincent, A.; Bashir, R. Point-of-care Sensors for the Management of Sepsis. *Nat. Biomed. Eng.* **2018**, *2*, 640−648.

(3) Pinalli, R.; Pedrini, A.; Dalcanale, E. Biochemical Sensing with Macrocyclic Receptors. *Chem. Soc. Rev.* **2018**, *47*, 7006−7026.

(4) Krämer, J.; Kang, R.; Grimm, L. M.; De Cola, L.; Picchetti, P.; Biedermann, F. Molecular Probes, Chemosensors, and Nanosensors for Optical Detection of Biorelevant Molecules and Ions in Aqueous Media and Biofluids. *Chem. Rev.* **2022**, *122*, 3459−3636.

(5) Freeman, W. A.; Mock, W. L.; Shih, N.-Y. Cucurbituril. *J. Am. Chem. Soc.* **1981**, *103*, 7367−7368.

(6) Kim, J.; Jung, I.-S.; Kim, S.-Y.; Lee, E.; Kang, J.-K.; Sakamoto, S. Y.; Kim, K. New Cucurbituril Homologues: Syntheses, Isolation, Characterization, and X-ray Crystal Structures of Cucurbit[n]uril (n = 5, 7, and 8). *J. Am. Chem. Soc.* **2000**, *122*, 540−541.

(7) Barrow, S. J.; Kasera, S.; Rowland, M. J.; del Barrio, J.; Scherman, O. A. Cucurbituril-Based Molecular Recognition. *Chem. Rev.* **2015**, *115*, 12320−12406.

(8) Buschmann, H.-J.; Jansen, K.; Schollmeyer, E. The Formation of Cucurbituril Complexes with Amino Acids and Amino Alcohols in Aqueous Formic Acid Studied by Calorimetric Titrations. *Thermochim. Acta* **1998**, *317*, 95−98.

(9) Hennig, A.; Bakirci, H.; Nau, W. M. Label-Free Continuous Enzyme Assays with Macrocycle-Fluorescent Dye Complexes. *Nat. Methods* **2007**, *4*, 629−632.

(10) Isobe, H.; Tomita, N.; Lee, J. W.; Kim, H.-J.; Kim, K.; Nakamura, E. Ternary Complexes Between DNA, Polyamine, and Cucurbituril: A Modular Approach to DNA-Binding Molecules. *Angew. Chem., Int. Ed.* **2000**, *39*, 4257−4260.

(11) Saleh, N.; Koner, A. L.; Nau, W. M. Activation and Stabilization of Drugs by Supramolecular pKa Shifts: Drug-Delivery Applications Tailored for Cucurbiturils. *Angew. Chem., Int. Ed.* **2008**, *47*, 5398−5401.

(12) Konda, S. K.; Maliki, R.; McGrath, S.; Parker, B. S.; Robinson, T.; Spurling, A.; Cheong, A.; Lock, P.; Pigram, P. J.; Phillips, D. R.; Wallace, L.; Day, A. I.; Collins, J. G.; Cutts, S. M. Encapsulation of Mitoxantrone within Cucurbit[8]uril Decreases Toxicity and Enhances Survival in a Mouse Model of Cancer. *ACS Med. Chem. Lett.* **2017**, *8*, 538−542.

(13) Biedermann, F.; Uzunova, V. D.; Scherman, O. A.; Nau, W. M.; De Simone, A. Release of High-Energy Water as an Essential Driving Force for the High-Affinity Binding of Cucurbit[n]urils. *J. Am. Chem. Soc.* **2012**, *134*, 15318−15323.

(14) Praetorius, A.; Bailey, D. M.; Schwarzlose, T.; Nau, W. M. Design of a Fluorescent Dye for Indicator Displacement from Cucurbiturils: A Macrocycle-Responsive Fluorescent Switch Operating through a pKa Shift. *Org. Lett.* **2008**, *10*, 4089−4092.

(15) Zhong, C.; Hu, C.; Kumar, R.; Trouillet, V.; Biedermann, F.; Hirtz, M. Cucurbit[n]uril-Immobilized Sensor Arrays for Indicator-Displacement Assays of Small Bioactive Metabolites. *ACS Appl. Nano Mater.* **2021**, *4*, 4676−4687.

(16) Sinn, S.; Spuling, E.; Bräse, S.; Biedermann, F. Rational Design and Implementation of a Cucurbit[8]uril-Based Indicator-Displacement Assay for Application in Blood Serum. *Chem. Sci.* **2019**, *10*, 6584−6593.

(17) Kumar, N. M.; Picchetti, P.; Hu, C.; Grimm, L. M.; Biedermann, F. Chemiluminescent Cucurbit[n]uril-Based Chemosensor for the Detection of Drugs in Biofluids. *ACS Sens.* **2022**, *7*, 2312−2319.

(18) Kumar, N. M.; Gruhs, P.; Casini, A.; Biedermann, F.; Moreno-Alcantar, G.; Picchetti, P. Electrochemical Detection of Drugs via a Supramolecular Cucurbit[7]uril-Based Indicator Displacement Assay. *ACS Sens.* **2023**, *8*, 2525−2532.

(19) Sinn, S.; Krämer, J.; Biedermann, F. Teaching Old Indicators even more Tricks: Binding Affinity Measurements with the Guest-Displacement Assay (GDA). *Chem. Commun.* **2020**, *56*, 6620−6623.

(20) Zhang, S.; Grimm, L.; Miskolczy, Z.; Biczók, L.; Biedermann, F.; Nau, W. M. Binding Affinities of Cucurbit[n]urils with Cations. *Chem. Commun.* **2019**, *55*, 14131−14134.

(21) Chinai, J. M.; Taylor, A. B.; Ryno, L. M.; Hargreaves, N. D.; Morris, C. A.; Hart, P. J.; Urbach, A. R. Molecular Recognition of Insulin by a Synthetic Receptor. *J. Am. Chem. Soc.* **2011**, *133*, 8810−8813.

(22) Lee, H. H.; Choi, T. S.; Lee, S. J.; Lee, J. W.; Park, J.; Ko, Y. H.; Kim, W. J.; Kim, K.; Kim, H. I. Supramolecular Inhibition of Amyloid Fibrillation by Cucurbit[7]uril. *Angew. Chem., Int. Ed.* **2014**, *53*, 7461−7465.

(23) Li, W.; Bockus, A. T.; Vinciguerra, B.; Isaacs, L.; Urbach, A. R. Predictive Recognition of Native Proteins by Cucurbit[7]uril in a Complex Mixture. *Chem. Commun.* **2016**, *52*, 8537−8540.

(24) Guagnini, F.; Engilberge, S.; Ramberg, K. O.; Perez, J.; Crowley, P. B. Engineered Assembly of a Protein-Cucurbituril Biohybrid. *Chem. Commun.* **2020**, *56*, 360−363.

(25) Liu, Y. H.; Zhang, Y. M.; Yu, H. J.; Liu, Y. Cucurbituril-Based Biomacromolecular Assemblies. *Angew. Chem., Int. Ed.* **2021**, *60*, 3870−3880.

(26) Saha, N. D.; Pradhan, S.; Sasmal, R.; Sarkar, A.; Berac, C. M.; Kolsch, J. C.; Pahwa, M.; Show, S.; Rozenholc, Y.; Topcu, Z.; Alessandrini, V.; Guibourdenche, J.; Tsatsaris, V.; Gagey-Eilstein, N.; Agasti, S. S. Cucurbit[7]uril Macrocyclic Sensors for Optical Fingerprinting: Predicting Protein Structural Changes to Identifying Disease-Specific Amyloid Assemblies. *J. Am. Chem. Soc.* **2022**, *144*, 14363−14379.

(27) Webber, M. J.; Appel, E. A.; Vinciguerra, B.; Cortinas, A. B.; Thapa, L. S.; Jhunjhunwala, S.; Isaacs, L.; Langer, R.; Anderson, D. G. Supramolecular PEGylation of biopharmaceuticals. *Proc. Natl. Acad. Sci. U.S.A.* **2016**, *113*, 14189−14194.

(28) Jones, L. M.; Super, E. H.; Batt, L. J.; Gasbarri, M.; Coppola, F.; Bhebhe, L. M.; Cheesman, B. T.; Howe, A. M.; Král, P.; Coulston, R.; Jones, S. T. Broad-Spectrum Extracellular Antiviral Properties of Cucurbit[n]urils. *ACS Infect. Dis.* **2022**, *8*, 2084−2095.

(29) Shaikh, M.; Mohanty, J.; Bhasikuttan, A. C.; Uzunova, V. D.; Nau, W. M.; Pal, H. Salt-induced guest relocation from a macrocyclic cavity into a biomolecular pocket: interplay between cucurbit[7]uril and albumin. *Chem. Commun.* **2008**, 3681−3683.

(30) Hu, C.; Grimm, L.; Prabodh, A.; Baksi, A.; Siennicka, A.; Levkin, P. A.; Kappes, M. M.; Biedermann, F. Covalent Cucurbit[7]-uril-Dye Conjugates for Sensing in Aqueous Saline Media and Biofluids. *Chem. Sci.* **2020**, *11*, 11142−11153.

(31) Hu, C.; Jochmann, T.; Chakraborty, P.; Neumaier, M.; Levkin, P. A.; Kappes, M. M.; Biedermann, F. Further Dimensions for Sensing in Biofluids: Distinguishing Bioorganic Analytes by the Salt-Induced

Adaptation of a Cucurbit[7]uril-Based Chemosensor. *J. Am. Chem. Soc.* **2022**, *144*, 13084−13095.

(32) Krämer, J.; Grimm, L. M.; Zhong, C.; Hirtz, M.; Biedermann, F. A supramolecular cucurbit[8]uril-based rotaxane chemosensor for the optical tryptophan detection in human serum and urine. *Nat. Commun.* **2023**, *14*, No. 518.

(33) Biedermann, F.; Ghale, G.; Hennig, A.; Nau, W. M. Fluorescent Artificial Receptor-Based Membrane Assay (FARMA) for Spatiotemporally Resolved Monitoring of Biomembrane Permeability. *Commun. Biol.* **2020**, *3*, 383.

(34) Nilam, M.; Karmacharya, S.; Nau, W. M.; Hennig, A. Proton-Gradient-Driven Sensitivity Enhancement of Liposome-Encapsulated Supramolecular Chemosensors. *Angew. Chem., Int. Ed.* **2022**, *61*, No. e202207950.

(35) Allen, T. M.; Cleland, L. G. Serum-Induced Leakage of Liposome Contents. *Biochim. Biophys. Acta* **1980**, *597*, 418−426.

(36) Laughlin, R. G. Equilibrium vesicles: fact or fiction? *Colloids Surf., A* **1997**, *128*, 27−38.

(37) Rideau, E.; Dimova, R.; Schwille, P.; Wurm, F. R.; Landfester, K. Liposomes and Polymersomes: A Comparative Review Towards Cell Mimicking. *Chem. Soc. Rev.* **2018**, *47*, 8572−8610.

(38) Barenholz, Y. Liposome Application: Problems and Prospects. *Curr. Opin. Colloid Interface Sci.* **2001**, *6*, 66−77.

(39) Discher, B. M.; Won, Y.-Y.; Ege, D. S.; Lee, J. C.-M.; Bates, F. S.; Discher, D. E.; Hammer, D. A. Polymersomes: Tough Vesicles Made from Diblock Copolymers. *Science* **1999**, *284*, 1143−1146.

(40) Dau, H.; Jones, G. R.; Tsogtgerel, E.; Nguyen, D.; Keyes, A.; Liu, Y. S.; Rauf, H.; Ordonez, E.; Puchelle, V.; Basbug Alhan, H.; Zhao, C.; Harth, E. Linear Block Copolymer Synthesis. *Chem. Rev.* **2022**, *122*, 14471−14553.

(41) Battaglia, G.; Ryan, A. J. Bilayers and Interdigitation in Block Copolymer Vesicles. *J. Am. Chem. Soc.* **2005**, *127*, 8757−8764.

(42) Canning, S. L.; Smith, G. N.; Armes, S. P. A Critical Appraisal of RAFT-Mediated Polymerization-Induced Self-Assembly. *Macromolecules* **2016**, *49*, 1985−2001.

(43) O'Reilly, R. K.; Joralemon, M. J.; Wooley, K. L.; J, H. C. Functionalization of Micelles and Shell Cross-linked Nanoparticles Using Click Chemistry. *Chem. Mater.* **2005**, *17*, 5976−5988.

(44) Rijpkema, S. J.; Langens, S.; van der Kolk, M. R.; Gavriel, K.; Toebes, B. J.; Wilson, D. A. Modular Approach to the Functionalization of Polymersomes. *Biomacromolecules* **2020**, *21*, 1853−1864.

(45) Napoli, A.; Boerakker, M. J.; Tirelli, N.; Nolte, R. J. M.; Sommerdijk, N. A. J. M.; Hubbell, J. A. Glucose-oxidase Based Self-Destructing Polymeric Vesicles. *Langmuir* **2004**, *20*, 3487−3491.

(46) Napoli, A.; Valentini, M.; Tirelli, N.; Müller, M.; Hubbell, J. A. Oxidation-Responsive Polymeric Vesicles. *Nat. Mater.* **2004**, *3*, 183−189.

(47) Lomas, H.; Canton, I.; MacNeil, S.; Du, J.; Armes, S. P.; Ryan, A. J.; Lewis, A. L.; Battaglia, G. Biomimetic pH Sensitive Polymersomes for Efficient DNA Encapsulation and Delivery. *Adv. Mater.* **2007**, *19*, 4238−4243.

(48) Cao, S.; Xia, Y.; Shao, J.; Guo, B.; Dong, Y.; Pijpers, I. A. B.; Zhong, Z.; Meng, F.; Abdelmohsen, L. K. E. A.; Williams, D. S.; van Hest, J. C. M. Biodegradable Polymersomes with Structure Inherent Fluorescence and Targeting Capacity for Enhanced Photo-Dynamic Therapy. *Angew. Chem., Int. Ed.* **2021**, *60*, 17629−17637.

(49) Sobotta, F. H.; Kuchenbrod, M. T.; Gruschwitz, F. V.; Festag, G.; Bellstedt, P.; Hoeppener, S.; Brendel, J. C. Tuneable Time Delay in the Burst Release from Oxidation-Sensitive Polymersomes Made by PISA. *Angew. Chem., Int. Ed.* **2021**, *60*, 24716−24723.

(50) Onaca, O.; Enea, R.; Hughes, D. W.; Meier, W. Stimuli-Responsive Polymersomes as Nanocarriers for Drug and Gene Delivery. *Macromol. Biosci.* **2009**, *9*, 129−139.

(51) Ou, B. S.; Saouaf, O. M.; Baillet, J.; Appel, E. A. Sustained delivery approaches to improving adaptive immune responses. *Adv. Drug Delivery Rev.* **2022**, *187*, No. 114401.

(52) Broz, P.; Driamov, S.; Ziegler, J.; Ben-Haim, N.; Marsch, S.; Meier, W.; Hunziker, P. Toward Intelligent Nanosize Bioreactors: A pH-Switchable, Channel-Equipped, Functional Polymer Nanocontainer. *Nano Lett.* **2006**, *6*, 2349−2353.

(53) Spulber, M.; Najer, A.; Winkelbach, K.; Glaied, O.; Waser, M.; Pieles, U.; Meier, W.; Bruns, N. Photoreaction of a Hydroxyalphenone with the Membrane of Polymersomes: A Versatile Method to Generate Semipermeable Nanoreactors. *J. Am. Chem. Soc.* **2013**, *135*, 9204−9212.

(54) Messager, L.; Burns, J. R.; Kim, J.; Cecchin, D.; Hindley, J.; Pyne, A. L.; Gaitzsch, J.; Battaglia, G.; Howorka, S. Biomimetic Hybrid Nanocontainers with Selective Permeability. *Angew. Chem., Int. Ed.* **2016**, *55*, 11106−11109.

(55) Varlas, S.; Foster, J. C.; Georgiou, P. G.; Keogh, R.; Husband, J. T.; Williams, D. S.; O'Reilly, R. K. Tuning the Membrane Permeability of Polymersome Nanoreactors Developed by Aqueous Emulsion Polymerization Induced Self Assembly. *Nanoscale* **2019**, *11*, 12643−12654.

(56) Liu, G.; Tan, J.; Cen, J.; Zhang, G.; Hu, J.; Liu, S. Oscillating the Local Milieu of Polymersome Interiors via Single Input-Regulated Bilayer Crosslinking and Permeability Tuning. *Nat. Commun.* **2022**, *13*, No. 585.

(57) Dinu, M. V.; Dinu, I. A.; Saxer, S. S.; Meier, W.; Pieles, U.; Bruns, N. Stabilizing Enzymes within Polymersomes by Coencapsulation of Trehalose. *Biomacromolecules* **2021**, *22*, 134−145.

(58) Rifaie-Graham, O.; Yeow, J.; Najer, A.; Wang, R.; Sun, R.; Zhou, K.; Dell, T. N.; Adrianus, C.; Thanapongpibul, C.; Chami, M.; Mann, S.; de Alaniz, J. R.; Stevens, M. M. Photoswitchable Gating of Non-Equilibrium Enzymatic Feedback in Chemically Communicating Polymersome Nanoreactors. *Nat. Chem.* **2023**, *15*, 110−118.

(59) van Dongen, S. F.; Nallani, M.; Cornelissen, J. J.; Nolte, R. J.; van Hest, J. C. A Three-Enzyme Cascade Reaction Through Positional Assembly of Enzymes in a Polymersome Nanoreactor. *Chem. − Eur. J.* **2009**, *15*, 1107−1114.

(60) Klermund, L.; Poschenrieder, S. T.; Castiglione, K. Biocatalysis in Polymersomes: Improving Multienzyme Cascades with Incompatible Reaction Steps by Compartmentalization. *ACS Catal.* **2017**, *7*, 3900−3904.

(61) Vriezema, D. M.; Garcia, P. M. L.; Sancho Oltra, N.; Hatzakis, N. S.; Kuiper, S. M.; Nolte, R. J. M.; Rowan, A. E.; van Hest, J. C. M. Positional Assembly of Enzymes in Polymersome Nanoreactors for Cascade Reactions. *Angew. Chem., Int. Ed.* **2007**, *46*, 7378−7382.

(62) van Oers, M. C. M.; Veldmate, W. S.; van Hest, J. C. M.; Rutjes, F. P. J. T. Aqueous Asymmetric Aldol Reactions in Polymersome Membranes. *Polym. Chem.* **2015**, *6*, 5358−5361.

(63) Ma, B. C.; Caire da Silva, L.; Jo, S. M.; Wurm, F. R.; Bannwarth, M. B.; Zhang, K. A. I.; Sundmacher, K.; Landfester, K. Polymer-Based Module for NAD(+) Regeneration with Visible Light. *ChemBioChem* **2019**, *20*, 2593−2596.

(64) Kim, J.; Kim, K. T. Polymersome-Based Modular Nanoreactors with Size-Selective Transmembrane Permeability. *ACS Appl. Mater. Interfaces* **2020**, *12*, 23502−23513.

(65) Madsen, J.; Canton, I.; Warren, N. J.; Themistou, E.; Blanazs, A.; Ustbas, B.; Tian, X.; Pearson, R.; Battaglia, G.; Lewis, A. L.; Armes, S. P. Nile Blue-Based Nanosized pH Sensors for Simultaneous Far-Red and Near-Infrared Live Bioimaging. *J. Am. Chem. Soc.* **2013**, *135*, 14863−14870.

(66) Yildiz, U. H.; De Hoog, H. P.; Fu, Z.; Tomczak, N.; Parikh, A. N.; Nallani, M.; Liedberg, B. Third-Party ATP Sensing in Polymersomes: A Label-Free Assay of Enzyme Reactions in Vesicular Compartments. *Small* **2014**, *10*, 442−447.

(67) Miller, A. J.; Pearce, A. K.; Foster, J. C.; O'Reilly, R. K. Probing and Tuning the Permeability of Polymersomes. *ACS Cent. Sci.* **2021**, *7*, 30−38.

(68) Sindelar, V.; Cejas, M. A.; Raymo, F. M.; Kaifer, A. E. Tight inclusion complexation of 2,7-dimethyldiazapyrenium in cucurbit[7]-uril. *New J. Chem.* **2005**, *29*, 280−282.

(69) Miskolczy, Z.; Megyesi, M.; Biczók, L.; Prabodh, A.; Biedermann, F. Kinetics and Mechanism of Cation-Induced Guest Release from Cucurbit[7]uril. *Chem. − Eur. J.* **2020**, *26*, 7433−7441.

(70) Byard, S. J.; Williams, M.; McKenzie, B. E.; Blanazs, A.; Armes, S. P. Preparation and Cross-Linking of All-Acrylamide Diblock Copolymer Nano-Objects via Polymerization Induced Self Assembly in Aqueous Solution. *Macromolecules* **2017**, *50*, 1482−1493.

(71) Zhou, W.; Qu, Q.; Xu, Y.; An, Z. Aqueous Polymerization-Induced Self-Assembly for the Synthesis of Ketone-Functionalized Nano-Objects with Low Polydispersity. *ACS Macro Lett.* **2015**, *4*, 495−499.

(72) Warren, N. J.; Armes, S. P. Polymerization-Induced Self-Assembly of Block Copolymer Nano-objects via RAFT Aqueous Dispersion Polymerization. *J. Am. Chem. Soc.* **2014**, *136*, 10174−10185.

(73) Rascol, O.; Fabbri, M.; Poewe, W. Amantadine in the Treatment of Parkinson's Disease and other Movement Disorders. *Lancet Neurol.* **2021**, *20*, 1048−1056.

(74) Nicholson, K. G.; Wiselka, M. J. Amantadine for Influenza A. *BMJ* **1991**, *302*, 425−426.

(75) Cheng, M. L.; Wang, C. H.; Shiao, M. S.; Liu, M. H.; Huang, Y. Y.; Huang, C. Y.; Mao, C. T.; Lin, J. F.; Ho, H. Y.; Yang, N. I. Metabolic Disturbances Identified in Plasma are Associated with Outcomes in Patients with Heart Failure: Diagnostic and Prognostic Value of Metabolomics. *J. Am. Coll. Cardiol.* **2015**, *65*, 1509−1520.

(76) Shah, P.; Swiatlo, E. A Multifaceted Role for Polyamines in Bacterial Pathogens. *Mol. Microbiol.* **2008**, *68*, 4−16.

(77) Hemmersbach, P.; Grosse, J. Nandrolone: A Multi-Faceted Doping Agent. *Handb. Exp. Pharmacol.* **2010**, *195*, 127−154.

(78) Moghaddam, S.; Yang, C.; Rekharsky, M.; Ko, Y. H.; Kim, K.; Inoue, Y.; Gilson, M. K. New Ultrahigh Affinity Host-Guest Complexes of Cucurbit[7]uril with Bicyclo[2.2.2]octane and Adamantane Guests: Thermodynamic Analysis and Evaluation of M2 Affinity Calculations. *J. Am. Chem. Soc.* **2011**, *133*, 3570−3581.

(79) Danysz, W.; Dekundy, A.; Scheschonka, A.; Riederer, P. Amantadine: Reappraisal of the Timeless Diamond-Target Updates and Novel Therapeutic Potentials. *J. Neural Transm.* **2021**, *128*, 127−169.

(80) Lee, E. C.; Kim, H. J.; Park, S. Y. Reversible Shape-Morphing and Fluorescence-Switching in Supramolecular Nanomaterials Consisting of Amphiphilic Cyanostilbene and Cucurbit[7]uril. *Chem. − Asian J.* **2019**, *14*, 1457−1461.

(81) Vissers, B.; Bohets, H.; Everaert, J.; Cool, P.; Vansant, E. F.; Du Prez, F.; Kauffmann, J. M.; Nagels, L. J. Characteristics of New Composite- and Classical Potentiometric Sensors for the Determination of Pharmaceutical Drugs. *Electrochim. Acta* **2006**, *51*, 5062−5069.

(82) Prabodh, A.; Sinn, S.; Grimm, L.; Miskolczy, Z.; Megyesi, M.; Biczók, L.; Bräse, S.; Biedermann, F. Teaching Indicators to Unravel the Kinetic Features of Host-Guest Inclusion Complexes. *Chem. Commun.* **2020**, *56*, 12327−12330.

(83) Kalicharan, R. W.; Bout, M. R.; Oussoren, C.; Vromans, H. Where Does Hydrolysis of Nandrolone Decanoate Occur in the Human Body after Release from an Oil Depot? *Int. J. Pharm.* **2016**, *515*, 721−728.

(84) Fallah-Araghi, A.; Meguellati, K.; Baret, J.-C.; El Harrak, A.; Mangeat, T.; Karplus, M.; Ladame, S.; Marques, C. M.; Griffiths, A. D. Enhanced Chemical Synthesis at Soft Interfaces: A Universal Reaction-Adsorption Mechanism in Microcompartments. *Phys. Rev. Lett.* **2014**, *112*, No. 028301.

(85) Lopez-Fontal, E.; Grochmal, A.; Foran, T.; Milanesi, L.; Tomas, S. Ship in a bottle: confinement-promoted self-assembly. *Chem. Sci.* **2018**, *9*, 1760−1768.

(86) Ginsberg, S.; Block, M. B.; Mako, M. E.; Rubenstein, A. H. Serum Insulin Levels Following Administration of Exogenous Insulin. *J. Clin. Endocrinol. Metab.* **1973**, *36*, 1175−1179.

(87) Rekharsky, M. V.; Mori, T.; Yang, C.; Ko, Y. H.; Selvapalam, N.; Kim, H.; Sobransingh, D.; Kaifer, A. E.; Liu, S.; Isaacs, L.; et al. A synthetic host-guest system achieves avidin-biotin affinity by overcoming enthalpy−entropy compensation. *Proc. Natl. Acad. Sci. U.S.A.* **2007**, *104*, 20737−20742.

(88) Wolfenden, R. Experimental Measures of Amino Acid Hydrophobicity and the Topology of Transmembrane and Globular Proteins. *J. Gen. Physiol.* **2007**, *129*, 357−362.

(89) Idili, A.; Parolo, C.; Ortega, G.; Plaxco, K. W. Calibration-Free Measurement of Phenylalanine Levels in the Blood Using an Electrochemical Aptamer-Based Sensor Suitable for Point-of-Care Applications. *ACS Sens.* **2019**, *4*, 3227−3233.

(90) Dinu, A.; Apetrei, C. A Review on Electrochemical Sensors and Biosensors Used in Phenylalanine Electroanalysis. *Sensors* **2020**, *20*, 2496.

(91) Gratton, S. E. A.; Ropp, P. A.; Pohlhaus, P. D.; Luft, J. C.; Madden, V. J.; Napier, M. E.; DeSimone, J. M. The Effect of Particle Design on Cellular Internalization Pathways. *Proc. Natl. Acad. Sci. U.S.A.* **2008**, *105*, 11613−11618.

(92) Najer, A.; Belessiotis-Richards, A.; Kim, H.; Saunders, C.; Fenaroli, F.; Adrianus, C.; Che, J.; Tonkin, R. L.; Høgset, H.; Lörcher, S.; Penna, M.; Higgins, S. G.; Meier, W.; Yarovsky, I.; Stevens, M. M. Block Length-Dependent Protein Fouling on Poly(2-oxazoline)-Based Polymersomes: Influence on Macrophage Association and Circulation Behavior. *Small* **2022**, *18*, No. 2201993.